



Cryptic CH₄ cycling in the sulfate–methane transition of marine sediments apparently mediated by ANME-1 archaea

F. Beulig¹ · H. Røy¹ · S.E. McGlynn² · B.B. Jørgensen¹

Received: 2 June 2018 / Revised: 10 August 2018 / Accepted: 17 August 2018 / Published online: 7 September 2018
© International Society for Microbial Ecology 2018

Abstract

Methane in the seabed is mostly oxidized to CO₂ with sulfate as the oxidant before it reaches the overlying water column. This microbial oxidation takes place within the sulfate–methane transition (SMT), a sediment horizon where the downward diffusive flux of sulfate encounters an upward flux of methane. Across multiple sites in the Baltic Sea, we identified a systematic discrepancy between the opposing fluxes, such that more sulfate was consumed than expected from the 1:1 stoichiometry of methane oxidation with sulfate. The flux discrepancy was consistent with an oxidation of buried organic matter within the SMT, as corroborated by stable carbon isotope budgets. Detailed radiotracer experiments showed that up to 60% of the organic matter oxidation within the SMT first produced methane, which was concurrently oxidized to CO₂ by sulfate reduction. This previously unrecognized “cryptic” methane cycling in the SMT is not discernible from geochemical profiles due to overall net methane consumption. Sedimentary gene pools suggested that nearly all potential methanogens within and beneath the SMT belonged to ANME-1 archaea, which are typically associated with anaerobic methane oxidation. Analysis of a metagenome-assembled genome suggests that predominant ANME-1 do indeed have the enzymatic potential to catalyze both methane production and consumption.

Introduction

Methane dynamics in the seabed are linked to mineralization of organic matter, which is mediated by complex microbial communities and coupled to the utilization of oxidants in a sequence that follows a progressive decrease in energy yield [1]. In most continental margin sediments sulfate reduction is the main pathway of anaerobic organic C oxidation [2]. When sulfate and other available electron acceptors are depleted at depth, the mineralization of

organic C proceeds to CH₄ and CO₂ [1, 3]. The flux of methane from the seabed to the overlying water column is controlled by sulfate-dependent anaerobic oxidation of methane (AOM) to CO₂ catalyzed by a syntrophic consortium of anaerobic methane oxidizing (ANME) archaea and sulfate reducing bacteria [4, 5]. Most AOM takes place within the sulfate-methane transition (SMT), a sediment interval where overlapping sulfate and methane drive a kinetically sluggish and thermodynamically poor AOM process [6–8].

The geochemical zonation in marine sediments is evident from major pore-water constituents, such as sulfate, methane, and dissolved inorganic carbon (DIC), but microbial processes behind this zonation are not as simple as they appear. A recent study identified a global imbalance of methane and sulfate fluxes into the SMT [9], and it is suggested that organoclastic sulfate reduction extends far into the SMT [10, 11]. This additional sulfate consumption may explain the apparently nonstoichiometric oxidation of methane by sulfate. Further, extremely ¹³C-depleted methane at the base of the SMT has been proposed to be the result of concurrent AOM and methanogenesis [12], or of C isotope equilibration between CH₄ and CO₂ during AOM under low sulfate supply [13]. It thus appears that other microbial processes in addition

Electronic supplementary material The online version of this article (<https://doi.org/10.1038/s41396-018-0273-z>) contains supplementary material, which is available to authorized users.

- ✉ F. Beulig
felix.beulig@bios.au.dk
- ✉ B.B. Jørgensen
bo.barker@bios.au.dk

¹ Department of Bioscience, Center for Geomicrobiology, Aarhus University, Ny Munkegade 114, Aarhus C, 8000, Denmark

² Earth-Life Science Institute, Tokyo Institute of Technology, Ookayama, Meguro-ku, Tokyo, 152–8551, Japan

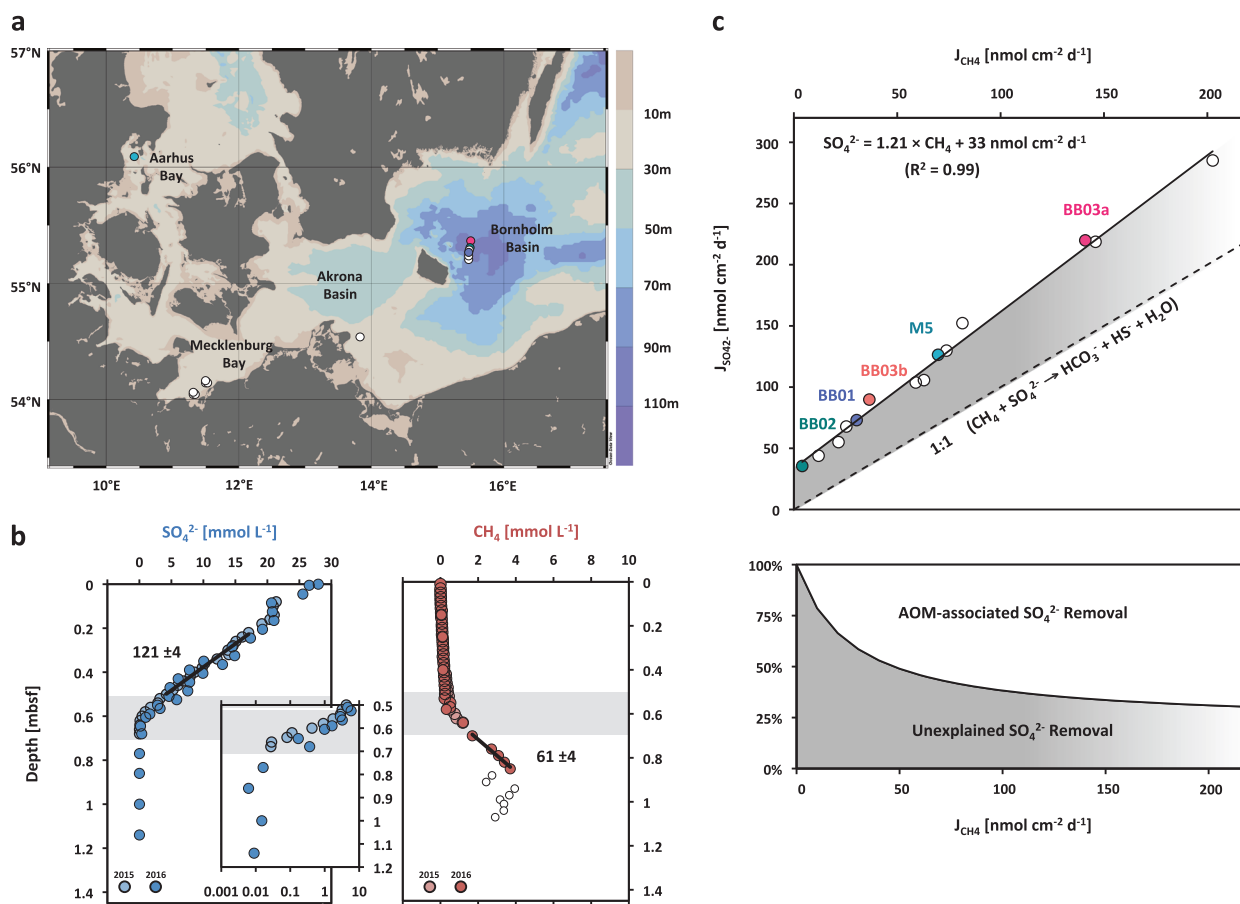


Fig. 1 **a** Sampling locations of Baltic Sea sites investigated in this study (Table S1). **b** Pore-water profiles of SO₄²⁻ and CH₄ concentrations in Aarhus Bay M5 sediment. The SO₄²⁻ is also shown with log₁₀ scale (inset). The gray shaded area indicates the sulfate-methane transition. Fluxes (in nmol cm⁻² d⁻¹) are reported next to the corresponding best-fit slope line used for calculation according to Fick's

first law (±standard error). Open circles indicate methane data points that are likely affected by degassing during sampling. **c** Total SO₄²⁻ and CH₄ fluxes into the SMT, as well as the fraction of those fluxes accounted for by AOM. Open circles represent data from the POS392 cruise (Fig. S1) [30]

to AOM may contribute to the carbon and sulfur transformations within the SMT.

Rates of microbial processes in sediments can be quantified by radiotracer experiments or mathematically from mass-balance and reaction–transport models, e.g., involving DIC and methane that are both released to the porewater during mineralization [14–16]. A combination of these approaches can resolve the spatial distribution and rate of individual microbial processes. Such methods have shown that rates of organic matter degradation decrease by a continuous power law function down through the sediment, irrespective of the prevailing redox zonation and terminal degradation pathway [17, 18].

Given the energy limitation that microorganisms experience under long-term conditions in the subseafloor [19, 20], the microbial communities may be balanced between the available energy flux and their minimum energy requirement [21]. Hence, the abundance of different functional groups

could be directly related to their total metabolic activity. Analyses of specific gene marker distributions may thereby locate associated microbial processes, and even identify “cryptic” reaction zones that are not directly discernible from geochemical analysis [22, 23]. Microorganisms involved in methane cycling can be studied via their functional genes, e.g., encoding the methyl-coenzyme M reductase (*mcr*), an enzyme unique to methanogens and anaerobic methane oxidizers. Methanogens have been difficult to detect in marine sediments, however, which has been attributed to their low abundance and to yet undiscovered methanogen groups with *mcr* genes that are not covered by available primer sets [24]. Even the ANME archaea themselves, which are phylogenetically related to methanogenic archaea but typically assumed to be obligate methane-oxidizers, might also be involved in methane formation [25–27].

The primary goal of this study was to understand microbial processes that affect C- and S-transformations

within the SMT. Specifically, we aimed to (i) constrain the quantitative relationship between AOM and other microbial processes that have major influence on CH_4 and SO_4^{2-} turnover in the SMT, and (ii) resolve the distribution of CH_4 production and consumption, as well as the microorganisms involved in these processes. We performed synoptic analyses of the biogeochemistry, microbial activity, and molecular biology in sediment cores from Aarhus Bay and used new and previously reported data sets from the Baltic Sea to test the general validity of our results (Fig. 1a, Table S1).

Materials and methods

Sediment coring and sampling

Cruises were undertaken with the R/V *Aurora*, to Aarhus Bay station M5 [28, 29] in 2015 and 2016. Additionally, we utilized sample material and published data from other organic-rich fine-grained sediments in the Baltic Sea, especially from the Bornholm Basin, for our analysis (Table S1, Fig. S1) [18, 30]. Coring and sampling procedures for Aarhus Bay, using a combination of Rumohr corer and gravity corer, were similar to those employed during cruises to Bornholm Basin and described in ref. [18].

Pore-water and sediment biogeochemical analyses

Methods for the quantification of pore water sulfate, methane, DIC, acetate, and sediment organic C (C_{org}) were performed as described in ref. [18]. Briefly, sulfate was measured by an IC-2500 ion chromatography system (Dionex Corporation); methane was measured using a Gas Chromatograph (GC, SRI Instruments 310C) with a flame ionization detector and the stable carbon isotopic composition of methane was determined using a coupled preconcentration GC/IRMS (isotope ratio mass spectrometer, Thermo Fisher Scientific DeltaVTM) [31]; DIC was determined on a Finnigan GasBench II (Thermo Fisher Scientific) and the stable carbon isotopic composition was determined with an IRMS [11]; acetate was analyzed by two-dimensional ion chromatography-mass spectrometry [32, 33]. The concentration and stable carbon isotopic composition of C_{org} were determined by an elemental analyzer (Thermo Fisher Scientific Flash EA 1112) coupled to an IRMS. The $\delta^{13}\text{C}$ values are reported vs. the Vienna Pee Dee Belemnite standard.

Stoichiometric ratios of DIC production during AOM and organic matter mineralization

AOM leads to DIC production in the SMT according to a 1:1 reaction stoichiometry: $\text{CH}_4 + \text{SO}_4^{2-} \rightarrow \text{HCO}_3^- + \text{HS}^- +$

H_2O . The reaction stoichiometry for organic matter mineralization, depends on the mean carbon oxidation state (ox): $\text{C}_{\text{org}} + [(4 - ox)/8] \text{SO}_4^{2-} \rightarrow \text{HCO}_3^- + [(4 - ox)/8] \text{H}_2\text{S}$ for organoclastic sulfate reduction; and $\text{C}_{\text{org}} \rightarrow [(4 + ox)/8] \text{CO}_2 + [(4 - ox)/8] \text{CH}_4$ for methanogenesis. The ox values for the sediments investigated in this study were calculated from parameter plots of DIC vs. SO_4^{2-} ($d\text{DIC}/d\text{SO}_4^{2-} = -[8/(4 - ox)] \times [D_{\text{SO}_4^{2-}}/D_{\text{DIC}}]$) (Fig. S2) [34].

Diffusive fluxes

Diffusive fluxes of pore water solutes were calculated from their concentration gradients using Fick's First Law:

$$J = -\varphi \times D_s \times dC/dz \quad (1)$$

where J is the diffusive flux, C the concentration, z the depth, D_s the whole-sediment diffusion coefficient, and φ the porosity. D_s was calculated from porosity and molecular diffusion coefficients of individual species, D_i , at 8 °C in situ temperature and salinity of 27 for Aarhus Bay sediments ($D_{\text{CH}_4} = 0.973 \text{ cm}^2 \text{ d}^{-1}$, $D_{\text{SO}_4^{2-}} = 0.554 \text{ cm}^2 \text{ d}^{-1}$, $D_{\text{HCO}_3^-} = 0.597 \text{ cm}^2 \text{ d}^{-1}$) or salinity of 15 for the Baltic Sea sediments ($D_{\text{CH}_4} = 1.08 \text{ cm}^2 \text{ d}^{-1}$, $D_{\text{SO}_4^{2-}} = 0.566 \text{ cm}^2 \text{ d}^{-1}$, $D_{\text{HCO}_3^-} = 0.609 \text{ cm}^2 \text{ d}^{-1}$), according to $D_s = D_i/(1 - \ln(\varphi^2))$ [15]. Note that the isotopic composition of carbon in a solute flux (DIC or CH_4) past a given depth in the sediment column is not the same as the isotopic composition of the solute at that depth. The isotopic composition of the flux can, however, be deduced from the slope of mixing-reaction plots where (solute concentration \times isotopic composition) is plotted as function of solute concentration (Figs. S3–S5) [10, 35]. All fluxes and their $\delta^{13}\text{C}$ values used for the following isotope mass balance calculations are summarized in Table S2.

Calculation of DIC sources in the SMT from DIC-fluxes and isotopes

The isotopic composition of DIC produced within the SMT regardless of its source ($\delta^{13}\text{C}_{\text{DIC,JSM T}}$) was calculated from the balance of isotopes diffusing into, and out of the SMT [10]:

$$\delta^{13}\text{C}_{\text{DIC,JSM T}} = (\delta^{13}\text{C}_{\text{DIC,JTop}} \times J_{\text{DIC,Top}} - \delta^{13}\text{C}_{\text{DIC,JBot}} \times J_{\text{DIC,Bot}}) / (J_{\text{DIC,Top}} - J_{\text{DIC,Bot}}) \quad (2)$$

where by $J_{\text{DIC,Top}}$ and $J_{\text{IC,Bot}}$ represent the DIC flux just above and below the SMT, respectively; $\delta^{13}\text{C}_{\text{DIC,JTop}}$ and $\delta^{13}\text{C}_{\text{DIC,JBot}}$ are $\delta^{13}\text{C}$ values of the two DIC fluxes. The investigated sediments were carbonate-poor [11, 36, 37], and therefore the influence of authigenic carbonate

precipitation on DIC budgets was assumed to be negligible. Once the isotopic composition of the mixed DIC from AOM and organoclastic mineralization within the SMT was calculated, then the relative contribution from the two sources that would give that mixture could be calculated from the known isotopic composition of DIC:

$$F_{\text{DIC,org}} = \frac{(\delta^{13}\text{C}_{\text{DIC,JAOM}} - \delta^{13}\text{C}_{\text{DIC,JSMT}})}{(\delta^{13}\text{C}_{\text{DIC,JAOM}} - \delta^{13}\text{C}_{\text{DIC,Jorg}})} \quad (3)$$

where by $F_{\text{DIC,org}}$ is the fraction of DIC-production in the SMT that must come from mineralization of organic material. $\delta^{13}\text{C}_{\text{DIC,JAOM}}$ is the $\delta^{13}\text{C}$ value of DIC produced by AOM assuming ~9‰ fractionation during oxidation of methane ($\delta^{13}\text{C}_{\text{DIC,AOM}} = \delta^{13}\text{C}_{\text{SMT,CH}_4} - 9\text{‰}$) [38, 39]. $\delta^{13}\text{C}_{\text{DIC,Jorg}}$ is the expected $\delta^{13}\text{C}$ value of DIC produced by organoclastic activity ($\delta^{13}\text{C}_{\text{DIC,Jorg}} = \delta^{13}\text{C}_{\text{SMT,Corg}}$). Alternatively, $F_{\text{DIC,org}}$ can be calculated from the part of the sulfate flux that was not accounted for by methane oxidation:

$$J_{\text{DIC,org}} = [8/(4 - ox)] \times (J_{\text{SO}_4^{2-}} - J_{\text{CH}_4}) \quad (4)$$

$$J_{\text{DIC,AOM}} = J_{\text{CH}_4} \quad (5)$$

$$F_{\text{DIC,org}} = J_{\text{DIC,org}} / (J_{\text{DIC,org}} + J_{\text{DIC,AOM}}) \quad (6)$$

To test the data for internal consistency, Eq. (3) can be rearranged to isolate $\delta^{13}\text{C}_{\text{DIC,JSMT}}$, and calculate which isotopic composition the calculated $F_{\text{DIC,org}}$ would lead to:

$$\delta^{13}\text{C}_{\text{DIC,JSMT}} = \delta^{13}\text{C}_{\text{DIC,JAOM}} - [(\delta^{13}\text{C}_{\text{DIC,JAOM}} - \delta^{13}\text{C}_{\text{DIC,Jorg}}) \times F_{\text{DIC,org}}] \quad (7)$$

Measurements of gross rates with radiotracers

Radiotracer-based experiments to measure: (a) sulfate reduction rates using [³⁵S]-labeled sulfate (SRR), (b) methanogenesis rates using [¹⁴C]-labeled DIC (MGR_{DIC}), (c) methanogenesis rates, and (d) acetate oxidation rates using [2-¹⁴C]-labeled acetate were performed as described before [18]. C oxidation rates were calculated from SRR and MGR based on the estimated stoichiometry of organic matter mineralization during sulfate reduction and methanogenesis ($r_{\text{C:SO}_4^{2-}} = r_{\text{C:CH}_4} = 8/(4 - ox) = 1.37$ and 1.46 for Bornholm Basin and Aarhus Bay M5 sediments, respectively) [34]:

$$\text{COR} = \left[\text{SRR} \times r_{\text{C:SO}_4^{2-}} \right] + [(MGR_{\text{DIC}} + MGR_{\text{Ac}}) \times r_{\text{C:CH}_4}] \quad (8)$$

Modeling of net CH₄ turnover from solute profiles

The depth distribution of net methane turnover in the sediment (ΣR_{CH_4}) was calculated from the balance of reaction and transport using the following equation [40]:

$$\Sigma R_{\text{CH}_4} = (\omega \times dC_{\text{CH}_4}/dz) - (\varphi \times D_s \times d^2C_{\text{CH}_4}/dz^2) \quad (9)$$

whereby ω is the sedimentation rate (0.14 cm y⁻¹), C_{CH_4} is the methane concentration, z is depth, D_{CH_4} is the molecular diffusion coefficient of methane (0.973 cm² d⁻¹), and φ is porosity. The first- and second-order derivatives, corresponding to diffusive transport and production or consumption, respectively, were estimated by fitting a smoothing cubic spline function to the methane concentration data. The degree of smoothing was kept at the minimum needed to filter out noise in the data.

Thermodynamic and kinetic calculations

These are described in detail in SI Materials and Methods.

DNA extraction

Subsamples for DNA extraction were collected with sterile cut-off 5-ml syringes from the same core sections as those for process rate measurements, and immediately stored at -80 °C. Aliquots of frozen sediment (0.2 g wet weight) were used for total DNA extraction, as described in SI Materials and Methods.

Quantitative PCR

The gene abundance of *dsrB*, *mcrA*, and archaeal and bacterial 16S rRNA in sediment DNA extract was determined by quantitative polymerase chain reaction (qPCR) using primer mixtures (Table S3) *dsrB*-F1a-h/*dsrB*-4RSI1a-f [41], *mcrA*-uniF/*mcrA*-uniR, *arc915Fmod*/*Arch958R* [42, 43], and *bac908F*/*bac1075R* [44], as described in SI Materials and Methods.

Illumina MiSeq sequencing and sequence analysis

DNA was amplified with 25 PCR amplification cycles, using primers (Table S3) specific to the *mcrA* gene (*mlasF*/*mlasR*) [45], and the hypervariable regions (V3–V6) of the archaeal 16S rRNA gene (*arc344Fmod*/*arc915R*) [46, 47], according to protocols provided in these references. MiSeq sequencing of the PCR products was performed according to the Illumina® “16S Metagenomic Sequencing Library Preparation” protocol. Quality control, denoising and sequence analysis of

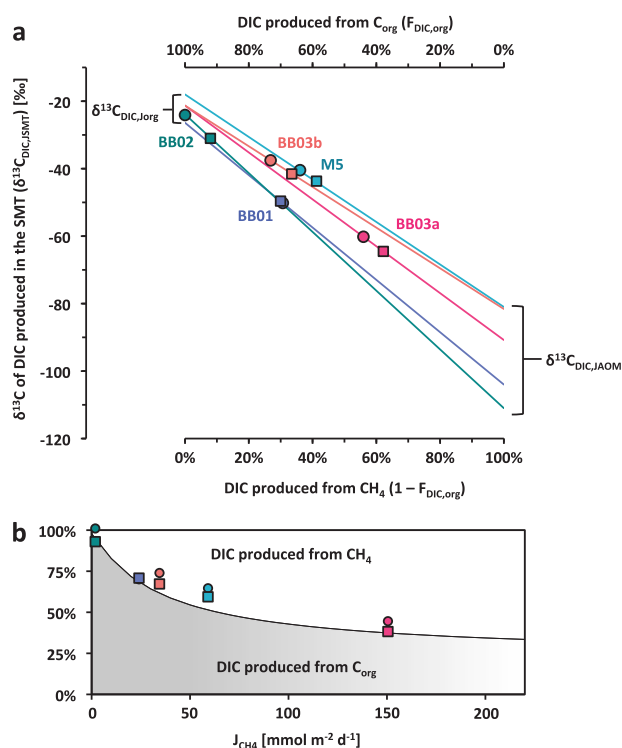


Fig. 2 **a** ^{13}C mass balance for the SMT in Aarhus Bay M5 and Bornholm Basin sediments. The diagonal lines show how the relative contributions of DIC produced from organoclastic activity ($F_{\text{DIC,org}}$) and from AOM ($1 - F_{\text{DIC,org}}$) shape the isotopic composition of the combined DIC product ($\delta^{13}\text{C}_{\text{DIC,JSMT}}$). The isotopic composition of DIC produced within the SMT was either calculated from the produced DIC (circles, Eqs. (2) and (3)), or the weighted average of the consumed substrates CH_4 and C_{org} (squares, Eqs. (6) and (7)). The closer the symbols plot the better the two independent mass balance models agree with each other. Lines and symbols are color coded similarly. Diffusive fluxes and isotopic values that were used for the mass balance calculations are summarized in Table S2. Biogeochemical profiles for the individual stations can be found in Figs. S3–S5. **b** Comparison of the CH_4 flux (J_{CH_4}) at individual stations with the fraction of DIC that accounted for oxidation of CH_4 or of C_{org} , as calculated from the isotopic composition of produced DIC (symbols as in **a**) or the SO_4^{2-} - CH_4 flux discrepancy (white and gray areas as in Fig. 1c)

paired-end MiSeq reads was performed with MOTHUR version 1.39.5 [48], fungene pipeline (<http://fungene.cme.msu.edu>) [49], and ARB version 6.0.4 [50], as described in detail in SI Materials and Methods.

Metagenome assembly, differential coverage binning, and metabolic reconstruction of the ANME-1 draft genome

Detailed information about the sampling procedure, DNA extraction, and sequencing of Aarhus Bay station M5 sediment metagenome samples can be found in ref. [51]. Metagenome reads were downloaded from the INSDC Sequence Read Archives (Bioproject ID PRJNA305566), and used for assembly, binning, and metabolic

reconstruction of an ANME-1 draft genome, as described in detail in SI Materials and Methods.

Results

Concentration profiles and diffusive fluxes of sulfate and methane

Sulfate concentrations in Aarhus Bay M5 sediment decreased almost linearly from ~ 26 mM at the sediment-water interface to < 100 μM in the SMT (Fig. 1b). Below the SMT sulfate concentrations were about 10 μM (inset in Fig. 1b). The sulfate profiles of other stations in the brackish Baltic Sea (Fig. S1) were similar in shape, but with lower values < 16 mM in surface sediments. Methane concentrations were generally low (< 0.01 mM) throughout the sulfate zone, and increased steeply down through the SMT and into the methane zone below (Fig. 1b and S1). In deeper parts of the methane zone scatter in the CH_4 concentration data often suggests extensive degassing of the supersaturated CH_4 , which was also visible upon core retrieval.

Diffusive fluxes of sulfate and methane were calculated by applying Fick's first law to linear gradients right above and below the SMT. In all investigated sediments, the sulfate flux down into the SMT exceeded the upwards methane flux, thereby deviating from the expected 1:1 ratio of AOM. The sulfate-to-methane flux ratio for the SMT in Aarhus Bay station M5 was 2.0, while the flux ratios in Bornholm Basin sediments ranged from 1.4 at BB03 to as high as 9.5 at BB02 (Fig. 1c). Comparison with highly depth-resolved sulfate and methane profiles obtained during the POS392 cruise to other sites in the Baltic Sea confirmed that this flux discrepancy was a general feature in the Baltic Sea. The relation between the sulfate and the methane flux could be described by the linear relationship $J_{\text{SO}_4^{2-}} = 1.21 J_{\text{CH}_4} + 0.33 \text{ mmol m}^{-2} \text{d}^{-1}$ ($R^2 = 0.99$), suggesting that (a) AOM is not the sole sulfate sink in the SMT, and (b) lower methane fluxes are, in these sediments, associated with a higher relative contribution of sulfate removal that is not driven by methane oxidation.

$\delta^{13}\text{C}$ budgets of DIC, CH_4 , and organic C for the SMT

We used two independent isotope mass balance approaches to identify the source of the DIC produced within the SMT ($\delta^{13}\text{C}_{\text{DIC,JSMT}}$; Eqs. (2)–(7)). We thereby utilized the extreme differences in $\delta^{13}\text{C}$ isotopic composition of C_{org} (-26.4 ‰ to -21.3 ‰ in Bornholm Basin and -17.2 ‰ in Aarhus Bay) and CH_4 (-81 ‰ to -101 ‰ in Bornholm Basin sediments and -84 ‰ in Aarhus Bay M5; Figs. S3–S5) as the substrates for organoclastic activity and AOM, respectively. A comparison of the two independent ways to calculate the relative contribution of organoclastic activity to

DIC production in the SMT ($F_{\text{DIC,org}}$) is shown in Fig. 2a. The two approaches agree well, and suggest DIC that is significantly enriched in ¹³C as compared to the δ¹³C isotopic signature of the upwards diffusing CH₄. Therefore, not only AOM, but also organoclastic activity appears to contribute substantially to C cycling within the SMT. The δ¹³C of produced DIC followed the trend of increasing influence of AOM in sediments with higher methane fluxes (Fig. 2b), consistent with the observed scaling of SO₄²⁻–CH₄ flux discrepancies (Fig. 1c). However, even at station BB03a, with shallowest SMT (0.23–0.51 mbsf) and highest methane flux (155 nmol cm⁻² d⁻¹), δ¹³C_{DIC,JSMT} values suggested that about 35% of the DIC produced in the SMT originated from C_{org} oxidation.

Vertical profiles of microbial activity

We resolved the vertical rate distribution of organoclastic SRR and MGR by radiotracer-based experiments, and determined their contribution to C transformations in the SMT. SRR were highest in the uppermost 5 cm (>100 nmol cm⁻³ d⁻¹ in Aarhus Bay M5 and >10 nmol cm⁻³ d⁻¹ in Bornholm Basin) (Fig. 3b) [18], and dropped in a log–log linear relationship with sediment depth down toward the SMT. MGR_{DIC} in the sulfate zone were only above detection limit beneath 40 cmbsf and were 2–3 orders of magnitude lower than SRR above the SMT (<10⁻¹ nmol cm⁻³ d⁻¹). Modeled rates of net CH₄ consumption were also <10⁻¹ nmol cm⁻³ d⁻¹ throughout the sulfate zone (Fig. 3a).

In the SMT, both SRR and MGR_{DIC} increased parallel to rates of net CH₄ consumption, with a distinct peak in the lower part of the SMT where sulfate concentrations dropped to low values <0.1 mM (Fig. 3a, b). Here, MGR_{DIC} were generally as high as or higher than corresponding SRR (Fig. S6). It is, therefore, unlikely that AOM-associated enzymatic back-reaction, leading to conversion of ¹⁴C-DIC to ¹⁴CH₄, represented a major component in our measurements.

In the methane zone, MGR_{DIC} continued to decrease along the same log–log linear depth trend that was found for SRR in the sulfate zone, whereas SRR dropped away from this trend. In all sampled depth intervals, MGR_{AC} were extremely low (<10⁻³ nmol cm⁻³ d⁻¹, Fig. 3b), and thereby accounted for <1% of the total CH₄ production. The [2-¹⁴C]-acetate was instead oxidized to CO₂ with rates similar in trend, but lower than, SRR in the sulfate zone, or MGR in the methane zone.

Profiles of prokaryotic abundance and methanogen diversity

Absolute and relative abundances of sulfate reducing and methane-cycling microbes in sediments of station M5 were investigated by qPCR of the genes encoding: (a) the β subunit of dissimilatory sulfite reductase (*dsrB*), (b) the α

subunit of methyl coenzyme M reductase (*mcrA*) covering most methanogens and the closely related ANME clades (Table S3). In addition, we estimated their relative abundance among the total microbial community by qPCR of archaeal and bacterial 16S rRNA genes. For this comparison, we assumed that on average the number of 16S rRNA gene copies per archaeal and bacterial genomes are 1 and 1.4, respectively [20].

All investigated gene markers showed vertical decrease in abundance, with ~10 times higher abundance at the sediment surface than at 1.25 mbsf (Fig. 4a). Consistent with the vertical distribution of methanogenesis rates, the proportion of *mcrA* genes showed a pronounced peak in the SMT with >5 × 10⁶ gene copies cm⁻³, accounting for up to ~10% of total archaea, and then dropped back to ~10⁶ gene copies cm⁻³, accounting for ~1% of total archaea in the methane zone below (Fig. 4b). *dsrB* gene abundance was highest close to the sediment surface with >5 × 10⁸ gene copies cm⁻³, accounting for ~20% of the bacterial 16S rRNA genes, and decreased throughout the core to ~1% of total bacteria.

We compared the abundance of putative methanogenic and sulfate reducing microbes with associated radiotracer-based metabolic activity measurement to calculate potential mean cell-specific metabolic rates (Fig. 4c). Sulfate reducer and methanogen genomes were hereby assumed to each contain a single copy of *dsrB* or *mcrA*, respectively, as indicated by available genome sequence data in public databases (<https://img.jgi.doe.gov> and <https://www.ncbi.nlm.nih.gov/genome/microbes/>). However, we note that prokaryotes may be polyploid, containing multiple genome copies [52–54]. Taking this into consideration, potential mean cell-specific metabolic rates indicated that, on the community level, sulfate reducers operated at fairly constant metabolic rates of ~0.4 fmol *dsrB*⁻¹ d⁻¹ throughout the sulfate zone with an abrupt decline to low values <0.01 fmol *dsrB*⁻¹ d⁻¹ under low sulfate concentrations in the methane zone. Here, potential mean cell-specific methanogenesis rates increased to average values of ~0.5 fmol *mcrA*⁻¹ d⁻¹, and were thereby similar to the potential cell-specific metabolic rates of sulfate reducers in the sulfate zone.

The diversity of putative methanogens and anaerobic methane oxidizers was assessed by high-throughput sequencing of *mcrA* genes as well as archaeal 16S rRNA genes. Phylogenetic reconstruction (Figs. 4d, e, and 6) suggests that the diverse group of methanogens in the sulfate zone belonged to, e.g. *Methanosarcinacea* (44–68%) or *Methanomicrobiaceae* (up to 22%). At the SMT, the community shifted to a complete dominance of ANME-1 archaea. Within the methane zone other putative methanogens remained largely undetected with amplicons for either the *mcr* or 16S rRNA genes. This suggests that ANME-1 archaea were not only involved in sulfate-dependent methane oxidation but possibly also in methanogenesis.

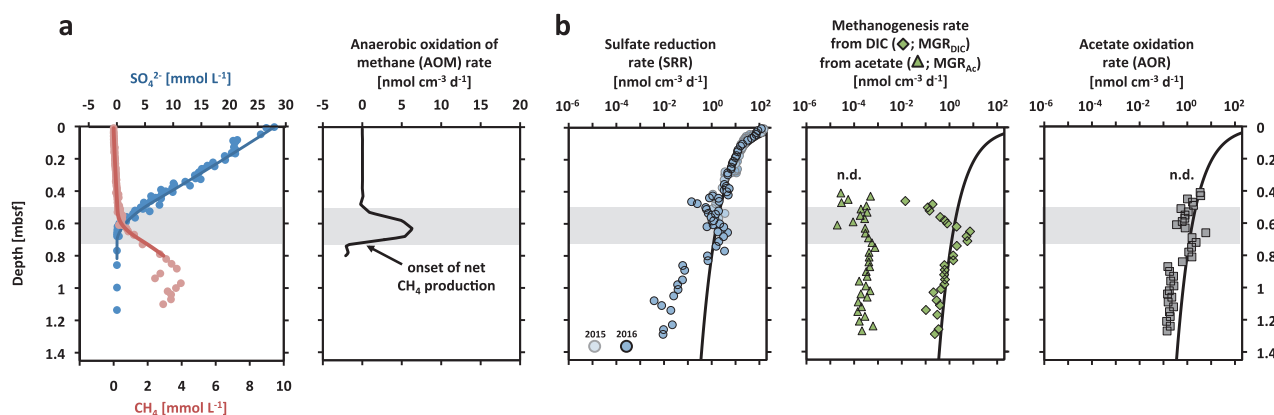


Fig. 3 **a** Depth profiles of sulfate and methane and of net methane consumption in Aarhus Bay M5 sediment modeled from a smoothing fit to the CH_4 concentration data (red curve). **b** Depth profiles of radiotracer-based microbial activity measurements in Aarhus Bay M5 sediment. The black curves indicate the trend of anaerobic C oxidation rates (COR), as calculated from the sum of SRR and MGR

(2016), corresponding to the following power law dependence on sediment depth (in cmbsf): $\text{COR} = 2930 \times \text{depth}^{-1.75} \text{ nmol C cm}^{-3} \text{ d}^{-1}$ ($N = 46$). The 95% confidence interval of the estimate of the exponent was -1.57 to -1.92 and the 95% confidence interval of the estimate of the constant was 1610 – 5540 . The gray shaded areas indicate the SMT. The sulfate reduction rate data are also shown in ref. [86]

Aarhus Bay Station M5 ANME-1 draft genome

In order to assess the metabolic potential of ANME-1 archaea, we extended our analysis of methanogenic marker genes to published metagenomic data sets that were generated from Aarhus Bay station M5 sediment [51]. Assembly and differential coverage binning [55, 56] of individual metagenomic libraries enabled the reconstruction of an ANME-1 draft genome (Fig. S7) that was, estimated from the abundance of single copy marker genes [57] to be $>86\%$ complete and with low potential for contamination ($<3\%$) (Table S4). The draft genome contained single copies of a 16S rRNA and *mcrA* gene that confirmed the affiliation with ANME-1 archaea (Fig. S8, Table S4). Nonetheless, it is possible that the binned contigs also include genetic information of other co-occurring and closely related ANME-1 organisms. Highest ANME-1 genome coverage was found for metagenome reads from 175 cmbsf, deep within the methane zone, and, consistent with our initial diversity screening, all *mcrA*-related genes that were detected in the individual metagenomic libraries showed high similarity to those from ANME-1 archaea (Fig. S8). Metabolic reconstruction of the ANME-1 draft genome revealed features that could potentially enable both methane oxidation and production, as discussed in the following.

Discussion

“Cryptic” methane cycling in the SMT

Our study provides multiple lines of evidence that upwards diffusing CH_4 is not the only electron donor driving SO_4^{2-} reduction in the SMT. Instead, a significant proportion of

SO_4^{2-} removal in the SMT is driven by the oxidation of buried organic matter, and this can occur either (i) directly via organoclastic sulfate reduction, or (ii) indirectly via methanogenesis, which provides an SMT-internal CH_4 source, thereby fueling additional AOM and generating a “cryptic methane cycle” (Fig. 5a).

Availability of sulfate in the SMT is limited by diffusive transport, and our results suggest that the competition between AOM and organoclastic sulfate reduction or methanogenesis is controlled by a balance between OM reactivity within the SMT and CH_4 flux into the SMT. The relatively higher contribution of AOM to overall SO_4^{2-} reduction in the SMT at sites with high methane fluxes is consistent with the predicted kinetic control of sulfate-dependent AOM in sediments, related to the high K_m for methane in the mM range [6]. High AOM rates appear to be restricted to a narrow zone in the lower part of the SMT where methane concentrations are high and SO_4^{2-} has not been depleted yet [7]. Indeed, the kinetic drive of AOM in Aarhus Bay M5 sediment increased towards a sharp peak at the base of the SMT (Fig. S9). Here, also the abundance of ANME-1, CH_4 consumption, and MGR_{DIC} peaked, indicating a tight coupling between methane oxidation and production in the same depth interval.

Taking into consideration that experimental rate measurements tend to scatter within an order of magnitude, we estimate that an important fraction of carbon cycling in the SMT is fueled by SMT-internal methanogenesis, accounting for 20% (station BB02) to 60% (station M5) of the total organoclastic activity (SRR + MGR) in this interval. This has a pronounced influence on the methane dynamics, as for example at station M5 the estimated methane turnover times in the SMT with and without this additional internal methane production were on average about 280 days and

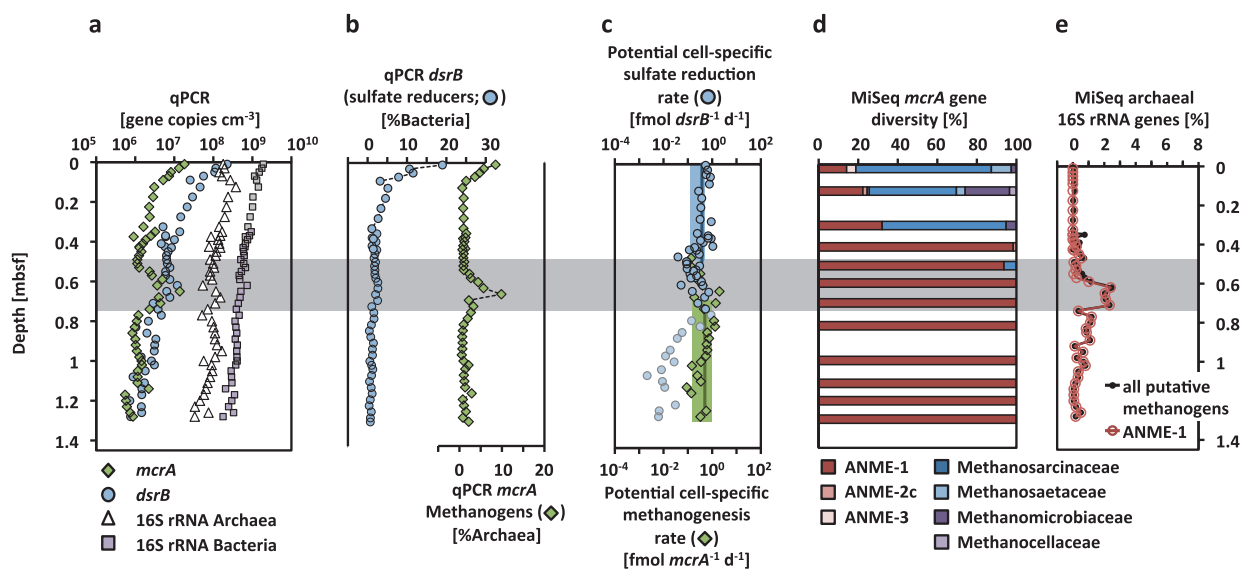


Fig. 4 **a, b** Depth profiles of absolute and relative prokaryotic abundances, **c** mean cell-specific metabolic rates, and **d, e** diversity of archaea potentially involved in methane cycling in Aarhus Bay M5 sediment. The vertical line in **c** depicts the average (\pm standard

deviation shown as shaded areas) of mean cell-specific sulfate reduction rates in the sulfate zone (blue) or mean cell-specific methanogenesis rates in the methane zone (green). The gray shaded area indicates the SMT

150 days, respectively (Fig. 5b). Our model of enhanced methane cycling by concurrent AOM and methanogenesis is consistent with observations of a distinct peak in experimentally measured methane oxidation rates at the base of the SMT and corroborates extremely ¹³C-depleted methane isotope signatures at the sulfate–methane transition [7, 12, 13]. The ¹³C-depleted DIC produced by AOM is hereby recycled back to methane with preferential use of ¹²C during CO₂ reduction.

The directly measured methanogenesis in the SMT of M5 (56 nmol CH₄ cm⁻² d⁻¹) was almost as high as the methanogenesis in the entire methane zone, as estimated from the methane flux (61 nmol CH₄ cm⁻² d⁻¹), and from extrapolation of the log–log linear depth trend of organoclastic activity (95 nmol CH₄ cm⁻² d⁻¹). Thus, a large fraction of the total methanogenesis in the sediment appears to take place through a “cryptic” methane cycle. This methane cycle has remained undetected by modeling of the net methane production from methane concentration data.

Metabolic potential of Aarhus Bay station M5 ANME-1 archaea

The evidence for concurrent methane production and oxidation in the same depth interval, presented above, together with amplicon and metagenomic data, suggest that one closely related group of organisms affiliated with ANME-1 are capable of both methane oxidation and methanogenesis. Previous studies that indicated the capability of ANME archaea to perform methanogenesis have been contemplated with doubt, however, because it remained unclear whether

methane production was instead attributed to other co-occurring methanogen populations [25, 58–60]. If we assume that other methanogens did not evade detection by our employed methods and represented <1% of detectable methanogens, their mean cell-specific metabolic rates would be 1–3 orders of magnitude higher than those of methanogens in, e.g., pure culture, enrichments, or different wetland soils (~0.05–5 fmol cell⁻¹ d⁻¹) [61–64], which would be highly unlikely. Although our results suggest that nearly all potential methanogens within and beneath the SMT of Aarhus Bay M5 sediments belonged to ANME-1 archaea, we cannot exclude that undiscovered methanogen lineages were also active. However, we consider this unlikely because (1) consistent with stable mean cell-specific metabolic rates of sulfate reducers in the sulfate zone, the abundance of ANME-1 in the SMT and in the methane zone closely reflected measured MGR, presumably in the absence of AOM, and (2) even the deeply sequenced metagenomes did not indicate presence of *mcr* genes belonging to putative methanogens other than ANME-1.

How could it be possible that ANME-1 are responsible for both methanogenesis and methane oxidation in the same sediment? Although ANME are commonly referred to as conducting a metabolism of “reverse methanogenesis” [65], the two physiologies differ in their terminal electron acceptors and protein complexes, which conserve energy as electrons move towards electron acceptors [26, 27]. Since ANME and methanogens are polyphyletic, different AOM and methanogenesis phenotypes may be distinguishable by phylogenetic clustering, but it is also possible that both physiologies could be found within a cluster. Alternatively,

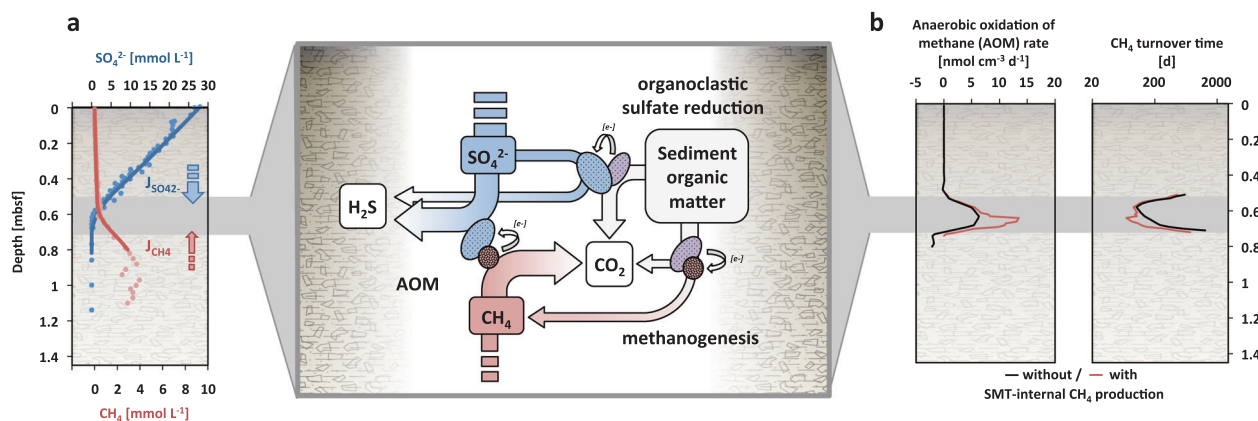


Fig. 5 a Proposed pathways of sulfate and methane turnover in the SMT. Co-occurrence of AOM and organoclastic activity results in an imbalance between SO₄²⁻ and CH₄ fluxes according to the reaction stoichiometry of organoclastic sulfate reduction and methanogenesis (cf. Materials and Methods). Because the produced CH₄ is consumed again by AOM, SMT-internal methanogenesis results in the same

additional sulfate consumption as would organoclastic sulfate reduction. Gray arrows indicate the transfer of reducing equivalents, symbolized by electrons [e⁻]. **b** CH₄ turnover in Aarhus Bay M5 sediment without and with SMT-internal methanogenesis. The gray shaded area indicates the SMT

the routing of electrons through different protein complexes could enable a switch between methanogenesis and methanotrophy in a single organism. The metabolic mode of ANME-1 cells could thereby be controlled by electron donor or acceptor availability, and also by syntrophic associations. Depending on whether the partner organisms are able to (a) accept reducing equivalents from the ANME-1 and use them to reduce sulfate, or (b) supply reducing equivalents that can be used by the ANME-1 to reduce CO₂, the net reaction would be either methane production or methane consumption. Such a metabolic versatility could provide a competitive advantage over other methanogens and, for example, allow ANME-1 archaea to adjust to seasonal variations in the depth of the SMT and the associated sulfate supply [66].

In the ANME-1 genome analyzed here, all core enzymatic carbon transfer and redox reactions required by a methanogenesis pathway were represented, even a N⁵,N¹⁰-methylene-tetrahydromethanopterin reductase (Mer) homolog that has not previously been detected in ANME-1 [65, 67, 68]. During anaerobic methanotrophy (Fig. 6a), generation of a proton gradient and ATP synthesis could be driven by complete reversal of the core methanogenic steps, coupling oxidation of CH₄ to CO₂ with transfer of the electrons to a partner organism [69]. As in previous ANME-1 genomes, HdrE was not detected [65, 67, 68], though here HdrD was. Electron transfer from the ANME-1 to a syntrophic partner might function via direct cell-to-cell connections, as indicated by the presence of genes encoding multihaem cytochrome complexes [69]. Although speculative, archaeal flagella/pilus-related proteins (Fla) might also play a role in direct electron transfer [70, 71]. Direct electron transfer from a different syntrophic partner to the ANME-1 could, in contrast, enable reduction of CO₂ to CH₄

(Fig. 6b). Cytoplasmic proton consumption during CO₂ reduction would result in a chemiosmotic potential that could be used for ATP generation. Alternatively, energy conservation may occur at the Mtr step. Although CO₂ reduction via direct electron transfer has been identified for other methanogens, the intracellular route of electrons and associated energetic constraints remain largely unresolved [72–74].

We identified several other potential electron entry points that could allow a methanogenic pathway in these ANME-1 cells. Consistent with previous studies of ANME, hydrogenases associated with hydrogenotrophic methanogenesis were largely absent [65, 67, 68]. The ANME-1 draft genome encoded only one putative hydrogenase with homology to membrane-associated [NiFe]-Group 4d hydrogenases [75, 76], suggestive of a possible route to supply reduced ferredoxin necessary for CO₂ reduction via H₂ oxidation at the expense of a chemiosmotic gradient via proton import. The reduction of F₄₂₀, an essential electron donor in methanogenesis from CO₂, might proceed through FrhB, the F₄₂₀-reducing hydrogenase subunit B. The FrhB would thereby facilitate electron exchange between ferredoxin and F₄₂₀, either alone or in combination with other enzyme complexes [77–79]. We found multiple gene copies of FrhB with a F₄₂₀ binding motif [79] in the ANME-1 draft genome that were co-located to genes encoding a cytoplasmic heterodisulfide reductase (HdrABC), and a putative membrane-bound Nuo-like oxidoreductase complex that shows structural similarity to F₄₂₀-H₂ dehydrogenase in *Methanosarcinales* [80].

We suspect that also other electron donors than H₂ could be used for CH₄ production, such as formate, carbon monoxide or acetate, as indicated by the presence of genes encoding a formate dehydrogenase (Fdo), and a CO

of $-10 \text{ kJ mol}_{\text{acetate}}^{-1}$ and -15 to $-20 \text{ kJ mol}_{\text{CH}_4}^{-1}$, respectively (Fig. S9).

Acknowledgments The research was funded by the Danish National Research Foundation Grant DNR104, the FP7 European Research Council (ERC) Advanced Grant 294200, the Danish Council for Independent Research Grant DFF—7014-00196 (to B.B.J.) and Danish Center for Marine Research Grant “Cryptic Biogeochemistry in the Bornholm Basin” (to H.R.). The authors thank captain Torben Vang and the crew of the R/V *Aurora* for sampling; Susanne Nielsen, Jeanette Pedersen, Britta Poulsen, and Karina Bomholt Oest for analytical work and technical support; André Pellerin, Angeliki Marietou, and Gilad Antler for help during sampling.

Author contributions F.B., H.R. and B.B.J. designed research. F.B. performed research and analyzed data. F.B. prepared the manuscript. S.E.M. contributed to the metabolic reconstruction of the ANME-1 genome. All co-authors commented on and provided substantial edits to the manuscript. B.B.J. and H.R. obtained the funding for this work.

Data availability Contig sequences of the ANME-1 draft genome have been deposited at the NCBI Sequence Read Archive (Whole Genome Submission) under BioProject ID PRJNA454851 with accession number QEXZ00000000. *mcrA* and 16S rRNA sequences have been deposited under the accession numbers SRR7119899–SRR7119910 and SRR716023–SRR7126072.

Compliance with ethical standards

Conflict of interest The authors declare that they have no conflict of interest.

References

- Jørgensen BB. Bacteria and Marine Biogeochemistry. Marine Geochemistry. Berlin, Heidelberg: Springer; 2006. p. 169–206.
- Jørgensen BB. Mineralization of organic matter in the sea bed—the role of sulphate reduction. *Nature*. 1982;296:643–5.
- McInerney MJ, Bryant MP. Basic principles of bioconversions in anaerobic digestion and methanogenesis. In: Sofer SS, Zaborsky OR, editors. Biomass conversion processes for energy and fuels. US: Springer; 1981. p. 277–96.
- Boetius A, Ravenschlag K, Schubert CJ, Rickert D, Widdel F, Gieseke A, et al. A marine microbial consortium apparently mediating anaerobic oxidation of methane. *Nature*. 2000;407:623–6.
- Orphan VJ, House CH, Hinrichs K-U, McKeegan KD, DeLong EF. Methane-consuming archaea revealed by directly coupled isotopic and phylogenetic analysis. *Science*. 2001;293:484–7.
- Katja N, Antje B, Martin K, Friedrich W. In vitro demonstration of anaerobic oxidation of methane coupled to sulphate reduction in sediment from a marine gas hydrate area. *Environ Microbiol*. 2002;4:296–305.
- Knab NJ, Dale AW, Lettmann K, Fossing H, Jørgensen BB. Thermodynamic and kinetic control on anaerobic oxidation of methane in marine sediments. *Geochim Cosmochim Acta*. 2008;72:3746–57.
- Hoehler TM, Alperin MJ, Albert DB, Martens CS. Field and laboratory studies of methane oxidation in an anoxic marine sediment: Evidence for a methanogen-sulfate reducer consortium. *Glob Biogeochem Cycles*. 1994;8:451–63.
- Egger M, Riedinger N, Mogollón JM, Jørgensen BB. Global diffusive fluxes of methane in marine sediments. *Nat Geosci*. 2018;11:421–25.
- Komada T, Burdige DJ, Li H-L, Magen C, Chanton JP, Cada AK. Organic matter cycling across the sulfate–methane transition zone of the Santa Barbara Basin, California Borderland. *Geochim Cosmochim Acta*. 2016;176:259–78.
- Flury S, Røy H, Dale AW, Fossing H, Tóth Z, Spiess V, et al. Controls on subsurface methane fluxes and shallow gas formation in Baltic Sea sediment (Aarhus Bay, Denmark). *Geochim Cosmochim Acta*. 2016;188:297–309.
- Borowski WS, Paull CK, Ussler W. Carbon cycling within the upper methanogenic zone of continental rise sediments: an example from the methane-rich sediments overlying the Blake Ridge gas hydrate deposits. *Mar Chem*. 1997;57:299–311.
- Yoshinaga MY, Holler T, Goldhammer T, Wegener G, Pohlman JW, Brunner B, et al. Carbon isotope equilibration during sulphate-limited anaerobic oxidation of methane. *Nat Geosci*. 2014;7:190–4.
- Jørgensen BB. A comparison of methods for the quantification of bacterial sulfate reduction in coastal marine sediments. *Geomicrobiol J*. 1978;1:11–27.
- Boudreau BP. Diagenetic models and their implementation: modelling transport and reactions in aquatic sediments, softcover reprint of the original 1st ed. 1997 edition. Berlin, Heidelberg: Springer-Verlag; 1997.
- Arndt S, Jørgensen BB, LaRowe DE, Middelburg JJ, Pancost RD, Regnier P. Quantifying the degradation of organic matter in marine sediments: a review and synthesis. *Earth-Sci Rev*. 2013;123:53–86.
- Middelburg JJ. A simple rate model for organic matter decomposition in marine sediments. *Geochim Cosmochim Acta*. 1989;53:1577–81.
- Beulig F, Røy H, Glombitza C, Jørgensen BB. Control on rate and pathway of anaerobic organic carbon degradation in the seabed. *Proc Natl Acad Sci*. 2018;115:367–72.
- Hoehler TM, Jørgensen BB. Microbial life under extreme energy limitation. *Nat Rev Microbiol*. 2013;11:83–94.
- Lever MA, Rogers KL, Lloyd KG, Overmann J, Schink B, Thauer RK, et al. Life under extreme energy limitation: a synthesis of laboratory- and field-based investigations. *FEMS Microbiol Rev*. 2015;39:688–728.
- LaRowe DE, Amend JP. Power limits for microbial life. *Front Microbiol*. 2015;6:718.
- Canfield DE, Stewart FJ, Thamdrup B, Brabandere LD, Dalsgaard T, Delong EF, et al. A cryptic sulfur cycle in oxygen-minimum-zone waters off the Chilean Coast. *Science*. 2010;330:1375–8.
- Holmkvist L, Ferdelman TG, Jørgensen BB. A cryptic sulfur cycle driven by iron in the methane zone of marine sediment (Aarhus Bay, Denmark). *Geochim Cosmochim Acta*. 2011;75:3581–99.
- Lever MA. A new era of methanogenesis research. *Trends Microbiol*. 2016;24:84–6.
- Lloyd KG, Alperin MJ, Teske A. Environmental evidence for net methane production and oxidation in putative ANaerobic METHanotrophic (ANME) archaea. *Environ Microbiol*. 2011;13:2548–64.
- McGlynn SE. Energy metabolism during anaerobic methane oxidation in ANME archaea. *Microbes Environ*. 2017;32:5–13.
- Timmers PHA, Welte CU, Koehorst JJ, Plugge CM, Jetten MSM, Stams AJM. Reverse methanogenesis and respiration in methanotrophic archaea. *Archaea*. 2017;2017:1654237.
- Langerhuus AT, Røy H, Lever MA, Morono Y, Inagaki F, Jørgensen BB, et al. Endospore abundance and d:l-amino acid modeling of bacterial turnover in holocene marine sediment (Aarhus Bay). *Geochim Cosmochim Acta*. 2012;99:87–99.
- Chen X, Andersen TJ, Morono Y, Inagaki F, Jørgensen BB, Lever MA. Bioturbation as a key driver behind the dominance of Bacteria over Archaea in near-surface sediment. *Sci Rep*. 2017;7:2400.

30. Jørgensen BB, Fossing H, Endler R. Chemistry of sediment cores of POSEIDON cruise POS392. 2011.
31. Rice AL, Gotoh AA, Ajie HO, Tyler SC. High-precision continuous-flow measurement of $\delta^{13}\text{C}$ and δD of atmospheric CH₄. *Anal Chem*. 2001;73:4104–10.
32. Glombitza C, Pedersen J, Røy H, Jørgensen BB. Direct analysis of volatile fatty acids in marine sediment porewater by two-dimensional ion chromatography-mass spectrometry. *Limnol Oceanogr Methods*. 2014;12:455–68.
33. Glombitza C, Jaussi M, Røy H, Seidenkrantz M-S, Lomstein BA, Jørgensen BB. Formate, acetate, and propionate as substrates for sulfate reduction in sub-arctic sediments of Southwest Greenland. *Front Microbiol* 2015;6:846.
34. Burdige DJ. *Geochemistry of marine sediments*. Princeton: Princeton University Press; 2006.
35. Sayles FL, Curry WB. $\delta^{13}\text{C}$, TCO₂, and the metabolism of organic carbon in deep sea sediments. *Geochim Cosmochim Acta*. 1988;52:2963–78.
36. Leipe T, Tauber F, Vallius H, Virtasalo J, Uścińowicz S, Kowalski N, et al. Particulate organic carbon (POC) in surface sediments of the Baltic Sea. *Geo-Mar Lett*. 2011;31:175–88.
37. Andrén E, Andrén T, Sohlenius G. The Holocene history of the southwestern Baltic Sea as reflected in a sediment core from the Bornholm Basin. *Boreas*. 2000;29:233–50.
38. Alperin MJ, Reeburgh WS, Whiticar MJ. Carbon and hydrogen isotope fractionation resulting from anaerobic methane oxidation. *Glob Biogeochem Cycles*. 1988;2:279–88.
39. Whiticar MJ. Carbon and hydrogen isotope systematics of bacterial formation and oxidation of methane. *Chem Geol*. 1999;161:291–314.
40. Berner RA. *Early diagenesis: a theoretical approach*. Princeton: Princeton University Press; 1980.
41. Lever MA, Rouxel O, Alt JC, Shimizu N, Ono S, Coggon RM, et al. Evidence for microbial carbon and sulfur cycling in deeply buried ridge flank basalt. *Science*. 2013;339:1305–8.
42. Cadillo-Quiroz H, Bräuer S, Yashiro E, Sun C, Yavitt J, Zinder S. Vertical profiles of methanogenesis and methanogens in two contrasting acidic peatlands in central New York State, USA. *Environ Microbiol*. 2006;8:1428–40.
43. Yu Y, Lee C, Hwang S. Analysis of community structures in anaerobic processes using a quantitative real-time PCR method. *Water Sci Technol J Int Assoc Water Pollut Res*. 2005;52:85–91.
44. Lever MA, Torti A, Eickenbusch P, Michaud AB, Šantl-Temkiv T, Jørgensen BB. A modular method for the extraction of DNA and RNA, and the separation of DNA pools from diverse environmental sample types. *Front Microbiol* 2015;6:476.
45. Steinberg LM, Regan JM. Phylogenetic comparison of the methanogenic communities from an acidic, oligotrophic Fen and an anaerobic digester treating municipal wastewater sludge. *Appl Environ Microbiol*. 2008;74:6663–71.
46. Stackebrandt E, Goodfellow M. *Nucleic acid techniques in bacterial systematics*. Chichester; New York, NY: Wiley; 1991.
47. Takai K, Horikoshi K. Rapid detection and quantification of members of the archaeal community by quantitative PCR using fluorogenic probes. *Appl Environ Microbiol*. 2000;66:5066–72.
48. Schloss PD, Westcott SL, Ryabin T, Hall JR, Hartmann M, Hollister EB, et al. Introducing mothur: open-source, platform-independent, community-supported software for describing and comparing microbial communities. *Appl Environ Microbiol*. 2009;75:7537–41.
49. Fish JA, Chai B, Wang Q, Sun Y, Brown CT, Tiedje JM, et al. FunGene: the functional gene pipeline and repository. *Front Microbiol* 2013;4:291.
50. Ludwig W, Strunk O, Westram R, Richter L, Meier H, kumar Y, et al. ARB: a software environment for sequence data. *Nucleic Acids Res*. 2004;32:1363–71.
51. Zaremba-Niedzwiedzka K, Caceres EF, Saw JH, Bäckström D, Juzokaite L, Vancaester E, et al. Asgard archaea illuminate the origin of eukaryotic cellular complexity. *Nature*. 2017;541:353–8.
52. Malandrín L, Huber H, Bernander R. Nucleoid structure and partition in *Methanococcus jannaschii*: an archaeon with multiple copies of the chromosome. *Genetics*. 1999;152:1315–23.
53. Hildenbrand C, Stock T, Lange C, Rother M, Soppa J. Genome Copy numbers and gene conversion in methanogenic archaea. *J Bacteriol*. 2011;193:734–43.
54. de Peer YV, Mizrahi E, Marchal K. The evolutionary significance of polyploidy. *Nat Rev Genet*. 2017;18:411–24.
55. Albertsen M, Hugenholtz P, Skarshewski A, Nielsen KL, Tyson GW, Nielsen PH. Genome sequences of rare, uncultured bacteria obtained by differential coverage binning of multiple metagenomes. *Nat Biotechnol*. 2013;31:533–8.
56. Karst SM, Kirkegaard RH, Albertsen M. mmgenome: a toolbox for reproducible genome extraction from metagenomes. *bioRxiv* 2016;059121.
57. Parks DH, Imelfort M, Skennerton CT, Hugenholtz P, Tyson GW. CheckM: assessing the quality of microbial genomes recovered from isolates, single cells, and metagenomes. *Genome Res*. 2015;25:1043–55.
58. Beth O, Vladimir S, Antje B, Samantha J. On the relationship between methane production and oxidation by anaerobic methanotrophic communities from cold seeps of the Gulf of Mexico. *Environ Microbiol*. 2008;10:1108–17.
59. Seifert R, Nauhaus K, Blumenberg M, Krüger M, Michaelis W. Methane dynamics in a microbial community of the Black Sea traced by stable carbon isotopes in vitro. *Org Geochem*. 2006;37:1411–9.
60. Wegener G, Krukenberg V, Ruff SE, Kellermann MY, Knittel K. Metabolic capabilities of microorganisms involved in and associated with the anaerobic oxidation of methane. *Front Microbiol* 2016;7:46.
61. Morozova D, Wagner D. Stress response of methanogenic archaea from Siberian permafrost compared with methanogens from nonpermafrost habitats. *FEMS Microbiol Ecol*. 2007;61:16–25.
62. Ma K, Conrad R, Lu Y. Responses of methanogen mcrA genes and their transcripts to an alternate dry/wet cycle of paddy field soil. *Appl Environ Microbiol*. 2012;78:445–54.
63. Yuan J, Ding W, Liu D, Kang H, Xiang J, Lin Y. Shifts in methanogen community structure and function across a coastal marsh transect: effects of exotic *Spartina alterniflora* invasion. *Sci Rep*. 2016;6:18777.
64. Lambrecht J, Cichocki N, Hübschmann T, Koch C, Harms H, Müller S. Flow cytometric quantification, sorting and sequencing of methanogenic archaea based on F420 autofluorescence. *Microb Cell Factor*. 2017;16:180.
65. Hallam SJ, Putnam N, Preston CM, Detter JC, Rokhsar D, Richardson PM, et al. Reverse methanogenesis: testing the hypothesis with environmental genomics. *Science*. 2004;305:1457–62.
66. Dale AW, Regnier P, Cappellen PV. Bioenergetic controls on anaerobic oxidation of methane (AOM) in coastal marine sediments: a theoretical analysis. *Am J Sci*. 2006;306:246–94.
67. Meyerdierks A, Kube M, Kostadinov I, Teeling H, Glöckner FO, Reinhardt R, et al. Metagenome and mRNA expression analyses of anaerobic methanotrophic archaea of the ANME-1 group. *Environ Microbiol*. 2010;12:422–39.
68. Stokke R, Roalkvam I, Lanzen A, Haflidason H, Steen IH. Integrated metagenomic and metaproteomic analyses of an ANME-1-dominated community in marine cold seep sediments. *Environ Microbiol*. 2012;14:1333–46.
69. McGlynn SE, Chadwick GL, Kempes CP, Orphan VJ. Single cell activity reveals direct electron transfer in methanotrophic consortia. *Nature*. 2015;526:531–5.

70. Shimoyama T, Kato S, Ishii S, Watanabe K. Flagellum mediates symbiosis. *Science*. 2009;323:1574.
71. Dubé C-D, Guiot SR. Direct interspecies electron transfer in anaerobic digestion: a review. *Biogas science and technology*. Cham: Springer; 2015. p. 101–15.
72. Rotaru A-E, Shrestha PM, Liu F, Shrestha M, Shrestha D, Embree M, et al. A new model for electron flow during anaerobic digestion: direct interspecies electron transfer to *Methanosaeta* for the reduction of carbon dioxide to methane. *Energy Environ Sci*. 2013;7:408–15.
73. Rotaru A-E, Shrestha PM, Liu F, Markovaite B, Chen S, Nevin KP, et al. Direct interspecies electron transfer between *Geobacter metallireducens* and *Methanosarcina barkeri*. *Appl Environ Microbiol*. 2014;80:4599–605.
74. Lovley DR. Syntrophy goes electric: direct interspecies electron transfer. *Annu Rev Microbiol*. 2017;71:643–64.
75. Søndergaard D, Pedersen CNS, Greening C. HydDB: a web tool for hydrogenase classification and analysis. *Sci Rep*. 2016;6:34212.
76. Sapra R, Verhagen MFJM, Adams MWW. Purification and characterization of a membrane-bound hydrogenase from the hyperthermophilic archaeon *Pyrococcus furiosus*. *J Bacteriol*. 2000;182:3423–8.
77. Arshad A, Speth DR, de Graaf RM, Op den Camp HJ, et al. A metagenomics-based metabolic model of nitrate-dependent anaerobic oxidation of methane by methanoperedens-like archaea. *Front Microbiol* 2015;6:1423.
78. Welte C, Deppenmeier U. Re-evaluation of the function of the F420 dehydrogenase in electron transport of *Methanosarcina mazei*. *FEBS J*. 2011;278:1277–87.
79. Welte C, Deppenmeier U. Bioenergetics and anaerobic respiratory chains of acetoclastic methanogens. *Biochim Biophys Acta*. 2014;1837:1130–47.
80. Baumer S, Ide T, Jacobi C, Johann A, Gottschalk G, Deppenmeier U. The F420H2 dehydrogenase from *Methanosarcina mazei* is a Redox-driven proton pump closely related to NADH dehydrogenases. *J Biol Chem*. 2000;275:17968–73.
81. Ragsdale SW, Pierce E. Acetogenesis and the Wood–Ljungdahl pathway of CO₂ fixation. *Biochim Biophys Acta Proteins Proteom*. 2008;1784:1873–98.
82. Drake HL, Küsel K, Matthies C. Acetogenic Prokaryotes. In: Rosenberg E, DeLong EF, Lory S, Stackebrandt E, Thompson F (eds). *The Prokaryotes*. Berlin, Heidelberg: Springer-Verlag; 2013. p. 3–60.
83. Basen M, Schut GJ, Nguyen DM, Lipscomb GL, Benn RA, Prybol CJ, et al. Single gene insertion drives bioalcohol production by a thermophilic archaeon. *Proc Natl Acad Sci*. 2014;111:17618–23.
84. Lang K, Schuldes J, Klingl A, Poehlein A, Daniel R, Brune A. New mode of energy metabolism in the seventh order of methanogens as revealed by comparative genome analysis of “*Candidatus Methanoplasma termitum*”. *Appl Environ Microbiol*. 2015;81:1338–52.
85. Evans PN, Parks DH, Chadwick GL, Robbins SJ, Orphan VJ, Golding SD, et al. Methane metabolism in the archaeal phylum Bathyarchaeota revealed by genome-centric metagenomics. *Science*. 2015;350:434–8.
86. Pellerin A, Antler G, Røy H, Findlay A, Beulig F, Scholze C, et al. The sulfur cycle below the sulfate–methane transition of marine sediments. *Geochim Cosmochim Acta*. 2018;239:74–89.